ARTICLES

Structure of the CED-4–CED-9 complex provides insights into programmed cell death in *Caenorhabditis elegans*

Nieng Yan[1], Jijie Chai[1], Eui Seung Lee[2,3], Lichuan Gu[1], Qun Liu[4], Jiaqing He[5], Jia-Wei Wu[1], David Kokel[2], Huilin Li[5], Quan Hao[4], Ding Xue[2] & Yigong Shi[1]

Interplay among four genes—*egl-1*, *ced-9*, *ced-4* and *ced-3*—controls the onset of programmed cell death in the nematode *Caenorhabditis elegans*. Activation of the cell-killing protease CED-3 requires CED-4. However, CED-4 is constitutively inhibited by CED-9 until its release by EGL-1. Here we report the crystal structure of the CED-4–CED-9 complex at 2.6 Å resolution, and a complete reconstitution of the CED-3 activation pathway using homogeneous proteins of CED-4, CED-9 and EGL-1. One molecule of CED-9 binds to an asymmetric dimer of CED-4, but specifically recognizes only one of the two CED-4 molecules. This specific interaction prevents CED-4 from activating CED-3. EGL-1 binding induces pronounced conformational changes in CED-9 that result in the dissociation of the CED-4 dimer from CED-9. The released CED-4 dimer further dimerizes to form a tetramer, which facilitates the autoactivation of CED-3. Together, our studies provide important insights into the regulation of cell death activation in *C. elegans*.

Genetic analyses in *C. elegans* led to the identification of four genes—*egl-1* (*egl*, for egg-laying defective), *ced-9* (*ced*, for cell-death abnormal), *ced-4* and *ced-3*—that collectively control the death of 131 somatic cells during hermaphrodite development[1,2] (Fig. 1a). The protein products of these four genes define a linear pathway. CED-3 is a caspase[3,4]: a cysteine-containing protease that cleaves its substrates after aspartate residues[5]. CED-3 is synthesized as an inactive zymogen. When cells are programmed to die, the CED-3 zymogen is thought to be activated by the adaptor molecule CED-4 (refs 6–11). In healthy cells, the pro-apoptotic protein CED-4 is sequestered by the mitochondria-bound protein CED-9 (refs 7, 10, 12–15), and thus is unable to activate CED-3. At the onset of cell death, the inhibitory CED-4–CED-9 interaction is disrupted by the pro-apoptotic protein EGL-1 (refs 16–19), which is transcriptionally activated in cells destined to die. The released CED-4 is thought to undergo homo-oligomerization, which then facilitates the activation of the CED-3 caspase[11].

The sequestration of CED-4 by CED-9 is essential for the regulation of programmed cell death in nematodes (Fig. 1a). However, it is not yet understood how CED-9 specifically recognizes the pro-apoptotic protein CED-4. It is also unclear how this recognition results in the inability of CED-4 to activate CED-3. In addition, despite some biochemical evidence[20], the mechanism by which EGL-1 releases CED-4 from the inhibitory CED-4–CED-9 complex remains unresolved. Last, but not least, the genetically identified pathway of CED-3 activation (Fig. 1a) has not been fully reconstituted *in vitro* using homogeneous recombinant proteins. In this study, we provide answers to these important questions using an integrated approach of structural biology, biochemistry, biophysics and genetics.

Structure of the CED-4–CED-9 complex

Assuming a 1:1 stoichiometry, the CED-4–CED-9 complex is predicted to exhibit a molecular weight of ~90 kDa. However, the apparent molecular weight of the complex always seemed to be ~150 kDa by gel filtration (see below). This complex, containing the full-length CED-4 and a transmembrane-segment-deleted CED-9 (residues 48–251), was crystallized. The structure was determined by multiple-wavelength anomalous dispersion (MAD) and refined at 2.6 Å resolution (Fig. 1b, Supplementary Table 1).

The structure shows an unexpected 2:1 stoichiometry between CED-4 and CED-9, accounting for the observed mass of ~150 kDa. The two molecules of CED-4, referred to as CED-4a and CED-4b, form an asymmetric dimer through an extensive interface involving a buried surface area of 4,167 Å^2 (Fig. 1b, c). Each CED-4 protein contains a bound ATP molecule and an associated magnesium ion. Only one CED-4 molecule, CED-4a, directly interacts with CED-9. CED-4a exhibits an elongated shape, with CED-9 and CED-4b binding to opposite sides (Fig. 1c). The carboxy-terminal helix of CED-9 protrudes from the CED-4–CED-9 complex; presumably, this arrangement allows convenient access of the CED-9 C-terminal transmembrane region to the mitochondrial outer membrane.

CED-4a comprises twenty-five α-helices and eight β-strands, which are organized into four sequential domains: an amino-terminal caspase recruitment domain (CARD; residues 1–105), a three-layered α/β-fold characteristic of the P-loop NTPases (residues 106–290), a helical domain (residues 291–370) and an extended winged-helix domain (residues 371–549) at the C terminus (Fig. 1 and Supplementary Fig. 1a). These four domains stack up closely against one another. CED-4b exhibits a similar structure, except that its CARD domain is flexible and disordered in the crystals.

[1]Department of Molecular Biology, Princeton University, Lewis Thomas Laboratory, Washington Road, Princeton, New Jersey 08544, USA. [2]Department of Molecular, Cellular and Developmental Biology, University of Colorado, Boulder, Colorado 80309, USA. [3]Department of Life Science, Gwangju Institute of Science and Technology, Gwangju 500-712, Republic of Korea. [4]Molecular Biology and Genetics, Cornell University, Ithaca, New York 14853, USA. [5]Biology Department, Brookhaven National Laboratory, Upton, New York 11973, USA.

The structure of CED-4 within the inhibitory CED-4–CED-9 complex exhibits a different domain organization compared to that of the autoinhibited apoptotic protease-activating factor 1 (Apaf-1; ref. 21), the mammalian homologue of CED-4 (ref. 22) (Supplementary Fig. 1b). In addition, the autoinhibited Apaf-1 is bound to ADP, but the CED-9-sequestered CED-4 is bound to ATP. Using the DALI server[23], the structures that are most homologous to CED-4 were found to be those of Cdc6 (ref. 24) and ORC2 (ref. 25), both ATPases belonging to the AAA+ (for ATPases associated with various cellular activities) family[26]. This analysis, in conjunction with an earlier report[27], identifies CED-4 as a member of the AAA+ family of ATPases.

Mechanism of CED-4 recognition by CED-9

The structure of the CED-4–CED-9 complex reveals the molecular basis by which CED-9 recognizes CED-4 (Fig. 2a, b). The recognition interface of CED-9 primarily involves the N-terminal segment (residues 67–79), the intervening loop between helices α3 and α4 (residues 143–147), and the α6 helix (residues 201–215). The N-terminal segment of CED-9 forms an extended loop, and stacks against the N-terminal portions of helices α2 and α4 and helix α8 of CED-4a (Fig. 2b). In this region, Asp 67 and Asp 79 in CED-9 each accept a pair of charge-stabilized hydrogen bonds from Arg 24 and Arg 117, respectively, in CED-4a. The α6 helix and the intervening loop between helices α3 and α4 in CED-9 interact with helix α11 and the following loop in CED-4a (Fig. 2b). Specifically, Arg 211 in CED-9 donates two hydrogen bonds to the backbone amide groups of Glu 214 and Asp 215 in CED-4a. Asn 212 in CED-9 also makes a hydrogen bond to Glu 52 in CED-4a. There are only a few van der Waals contacts at the CED-4a–CED-9 interface; these occur between the α3–α4 intervening loop in CED-9 and helix α11 and the following loop in CED-4a (Fig. 2b).

The CED-4a–CED-9 interactions seem to be ideal for their functional regulation. The extensive interface, involving 3,550 Å^2 of buried surface area and 13 hydrogen bonds, provides exquisite recognition specificity between CED-4a and CED-9. Nonetheless, the shape complementarity at the interface is poor (Supplementary Fig. 2a). A large proportion of the buried amino acids at the interface are not involved in intermolecular interactions. These structural features make it easier for EGL-1 to release CED-4 from the CED-4–CED-9 complex.

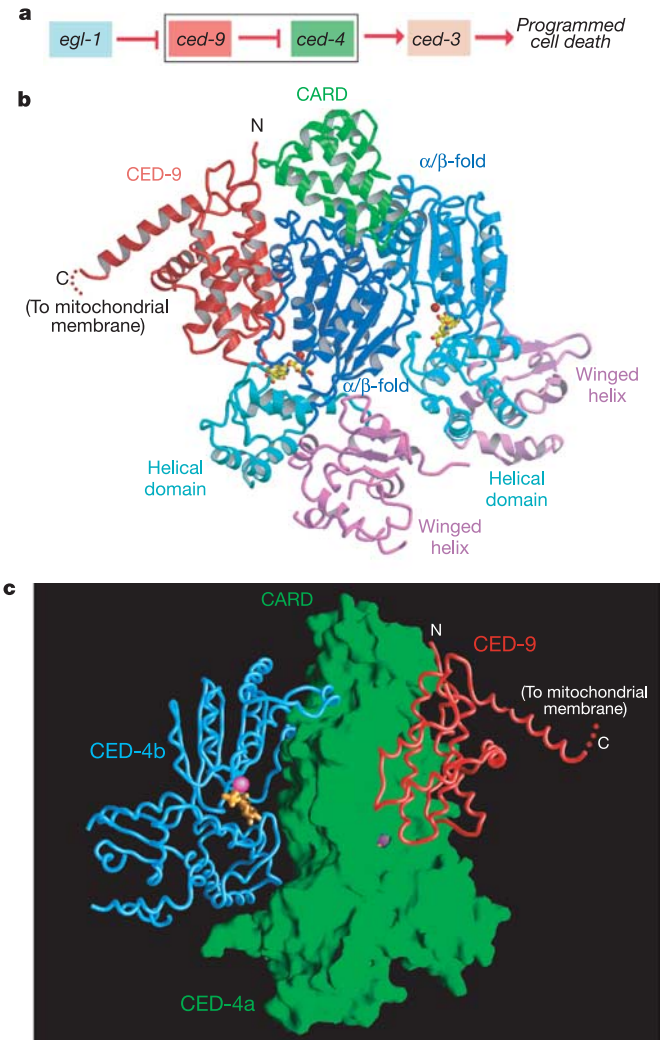

Figure 1 | Overall structure of the CED-4–CED-9 complex. a, A linear pathway of programmed cell death in *C. elegans*. **b**, Overall structure of the CED-4–CED-9 complex. Each CED-4 molecule comprises four sequential domains—CARD domain (green), α/β-fold (blue), helical domain (cyan) and winged-helix domain (magenta)—and contains a bound ATP molecule and a magnesium ion. **c**, Another view of the 2:1 CED-4–CED-9 complex. CED-4a (green) is shown as a surface representation. The bound ATP molecules and magnesium ions are highlighted in orange and magenta, respectively. Figures were prepared using MOLSCRIPT (ref. 39) and GRASP (ref. 40).

Mechanism of CED-4 release by EGL-1

The structure of CED-9 in the CED-4–CED-9 complex is similar to that of isolated CED-9 (ref. 28), with an overall root mean square deviation (r.m.s.d.) of 0.7 Å, but it is quite different from that of CED-9 in the EGL-1–CED-9 complex[20]. Comparison of the structure of the CED-4–CED-9 complex with that of the EGL-1–CED-9 complex[20] shows the molecular mechanism by which EGL-1 releases CED-4 from the inhibitory CED-4–CED-9 complex. The structural elements of CED-9 that directly bind to CED-4 are different from those that directly contact EGL-1 (Fig. 2c). However, the binding of EGL-1 to CED-9 is predicted to trigger pronounced conformational changes in CED-9 that result in the disruption of the interactions between CED-9 and CED-4a. On binding of EGL-1, the α4 helix of CED-9 is translocated towards CED-4a by as much as 6 Å (Supplementary Fig. 2b), which is predicted to cause a steric clash between CED-9 and CED-4a. In addition, four amino acids in CED-9 that are important for binding to CED-4 exhibit quite different side-chain and main-chain conformations upon binding to EGL-1 (Supplementary Fig. 2c). These altered conformations are no longer compatible for interaction with CED-4.

The binding affinity between CED-4 and CED-9 was estimated to be 48 ± 8 nM. In contrast, EGL-1 binds to CED-9 with a dissociation constant of approximately 6 nM (ref. 20). The stronger interaction between EGL-1 and CED-9 allows EGL-1 to bind to the CED-4-bound CED-9, and to dissociate CED-4 by inducing conformational changes in CED-9. To quantify this process directly, we titrated EGL-1 protein into pre-formed wild-type CED-4–CED-9 complex using isothermal titration calorimetry (ITC). EGL-1 efficiently dissociated CED-4 from the CED-4–CED-9 complex, with an apparent dissociation constant of 98 ± 18 nM (Fig. 2d).

CED-4a–CED-4b interface and ATP binding

One unexpected finding of this study is that a single CED-9 molecule binds to an asymmetric dimer of CED-4. The two molecules of CED-4 associate with each other mainly through van der Waals contacts (Fig. 3a, b). The asymmetric interaction results in the formation of an additional α-helix (α11b) in CED-4b that packs against CED-4a (Fig. 3b and Supplementary Fig. 1a). The interface between CED-4a and CED-4b consists of a primary and a secondary binding surface (Fig. 3a). In the primary interface, helices α8, α11 and α11b, all from the α/β-fold of CED-4b, pack against the CARD and α/β domains of

CED-4a (Fig. 3b). In the secondary area of contact, several residues from the helical domain of CED-4b make hydrogen bonds and salt bridges to the winged-helix domain of CED-4a.

Using mutagenesis, we tried to disrupt selectively the CED-4 dimer. Because of the extensive CED-4a–CED-4b interface, single point mutations only weakened, and failed to disrupt, their interactions (Supplementary Table 2). A CED-4 triple mutant, containing V230D, R233E and M234E amino-acid substitutions in helix α12 (Fig. 3b), abolished formation of the CED-4 dimer and, consequently, formed an apparent 1:1 complex with CED-9 as determined by gel filtration (Supplementary Fig. 3a).

CED-4a and CED-4b have a similar structure, with an r.m.s.d. of 0.8 Å over 359 aligned Cα atoms (Supplementary Fig. 3b). However, the CARD domain of CED-4a adopts a rigid conformation through interactions with the α/β-fold of CED-4b and CED-9, whereas the CARD domain of CED-4b is disordered in the crystals. Modelling studies show a severe steric clash if the CARD domain of CED-4b were to assume the same conformation as that of CED-4a. This analysis explains why CED-4b does not bind to CED-9: the CARD domain of CED-4b cannot adopt the same conformation that is required for interacting with CED-9, and the α/β domain of CED-4b already uses a similar interface, which would be required for binding to CED-9, for interacting with CED-4a.

ATP and magnesium are largely buried in both CED-4 molecules (Fig. 3c). ATP binds along the hinge region between the α/β domain and the helical domain. The specific coordination of ATP is achieved by a total of eleven hydrogen bonds, ten of which are directed towards the phosphate groups (Fig. 3d). Only one specific hydrogen bond is made to the adenine base, with the N6 atom of ATP donating a hydrogen bond to the backbone amide of Tyr 131. It is important to note that this hydrogen bond dictates the specificity for adenine over guanine, as the O6 atom of guanine is unable to interact with an amide oxygen atom. The γ-phosphate group is coordinated by three hydrogen bonds from Lys 165 (in the P-loop), Arg 273 and Tyr 369 (Fig. 3d). The magnesium ion is bound by the β- and γ-phosphates, and by the side chain of Ser 166 in the P-loop.

Notably, the CED-4–CED-9 complex showed no detectable ATPase activity. This is probably due to the structural arrangement in the vicinity of the γ-phosphate, which does not allow a general base to activate a water molecule. The closest general base, Asp 251 in the Walker B box, accepts a pair of charge-stabilized hydrogen bonds from Arg 380 (Fig. 3d). The closest distance between the carboxylate

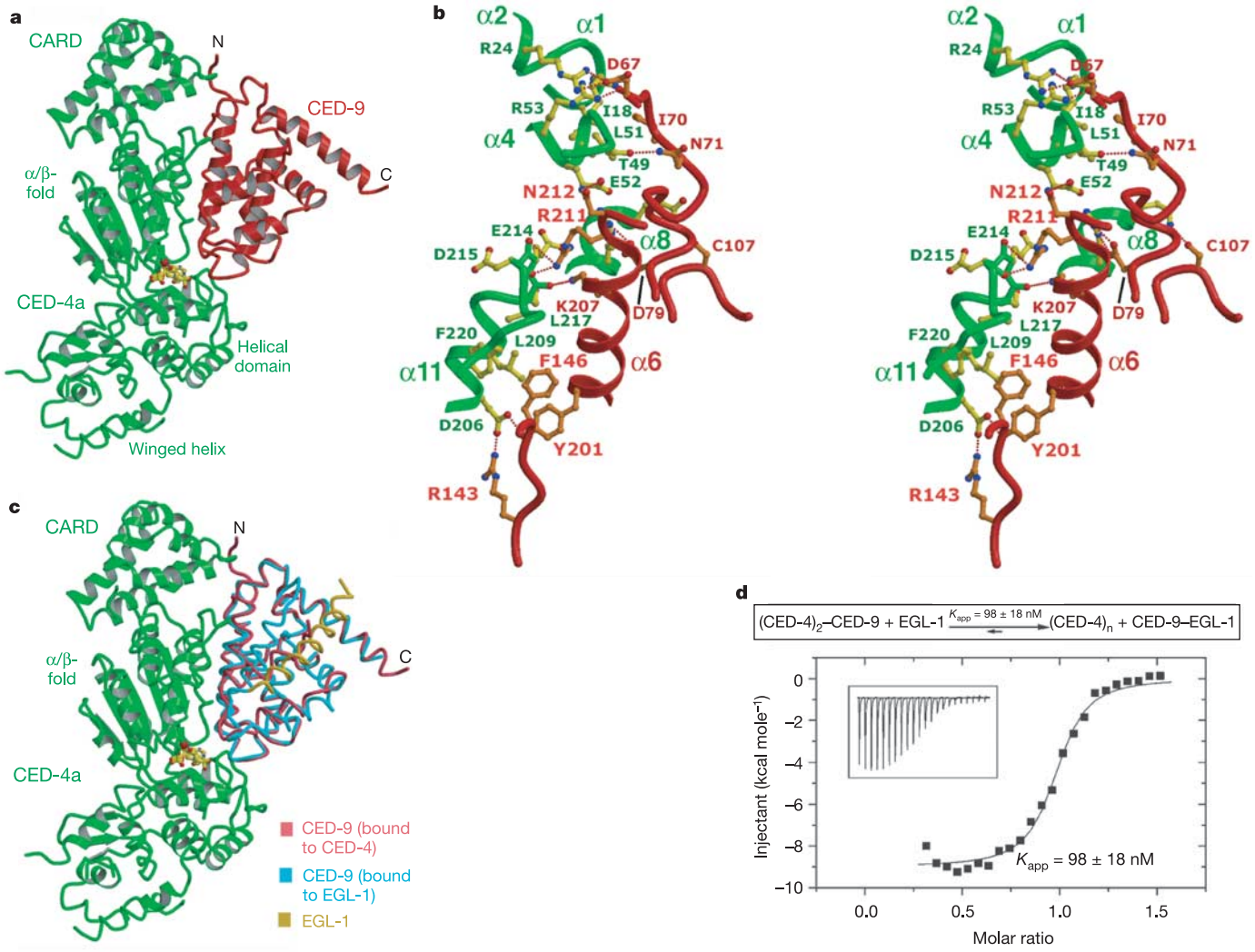

Figure 2 | Mechanisms of CED-4 recognition by CED-9, and CED-4 release by EGL-1. a, CED-9 binds to the CARD domain and the α/β-fold of CED-4a. **b**, A stereo view of the specific recognition between CED-4a (green) and CED-9 (red). Hydrogen bonds are shown as red dashed lines. The side chains from CED-4a and CED-9 are shown in yellow and orange, respectively. **c**, Structural superposition of CED-4-bound CED-9 with EGL-1-bound CED-9. EGL-1 binding triggers a conformation change in CED-9 that destabilizes the CED-4–CED-9 interactions. **d**, EGL-1 releases CED-4 from the CED-4–CED-9 complex. An apparent dissociation constant of 98 ± 18 nM was derived from ITC experiments.

side chain of Asp 251 and the γ-phosphorous atom is greater than 6 Å.

Tetramerization of CED-4

EGL-1 binding to CED-9 results in the release of CED-4 from the inhibitory CED-4–CED-9 complex. It is unclear whether the released CED-4 dimer directly facilitates CED-3 activation, or whether it requires an additional step of oligomerization. To address this, we incubated the wild-type CED-4–CED-9 complex with excess EGL-1 and performed gel filtration analysis. CED-4 was eluted at a volume corresponding to a molecular weight of approximately 250 kDa (Fig. 4a, red line), about twice that of the CED-4 dimer. This result suggested that the released CED-4 dimer may undergo further dimerization.

To characterize the putative CED-4 tetramer, we examined its morphology by electron microscopy (Fig. 4b). About 9,500 raw individual particle images were manually, but non-discriminatorily, selected from electron micrographs. These particles were subjected to reference-free classification into 188 classes through a multivariant statistical analysis. The use of a large class number ensured that particles of different views were not assigned into the same class. Particles within the same class were averaged to provide statistically defined views. Three averages, related by an in-plane rotation, showed an apparent four-fold symmetry with a dimension of 13 nm (Fig. 4b). All other class averages, as anticipated, represented views of the tetramer with various degrees of out-of-plane tilt. No class average with three-, five- or six-fold symmetry was observed. These observations provide strong evidence that the released CED-4 dimer undergoes an additional step of dimerization.

Reconstitution of the CED-3 activation pathway

Despite strong genetic evidence, the cell death pathway from EGL-1 to CED-3 (Fig. 1a) has not been reconstituted *in vitro* using homogeneous recombinant proteins. We determined whether CED-4, CED-9 and EGL-1 can collectively control the activation of the CED-3 zymogen *in vitro*. We purified full-length wild-type CED-4, transmembrane-segment-deleted CED-9 (residues 1–251 and 48–251), and full-length (residues 1–91) and truncated EGL-1 (residues 31–87) (Fig. 5a). We also purified a stoichiometric CED-4–CED-9 complex and a monomeric CED-4 mutant (Fig. 5a).

The wild-type CED-3 zymogen, generated by *in vitro* translation, was slowly autoprocessed as previously reported[9,29] (Fig. 5b, lanes 1–3). The autoprocessing requires the catalytic residue Cys 358, as the mutation C358S abolished CED-3 autoactivation (Fig. 5b, lanes 4 and 5). This result indicates that the processing of the CED-3 zymogen is not due to other contaminating protease(s). We first examined whether the recombinant full-length CED-4 protein can

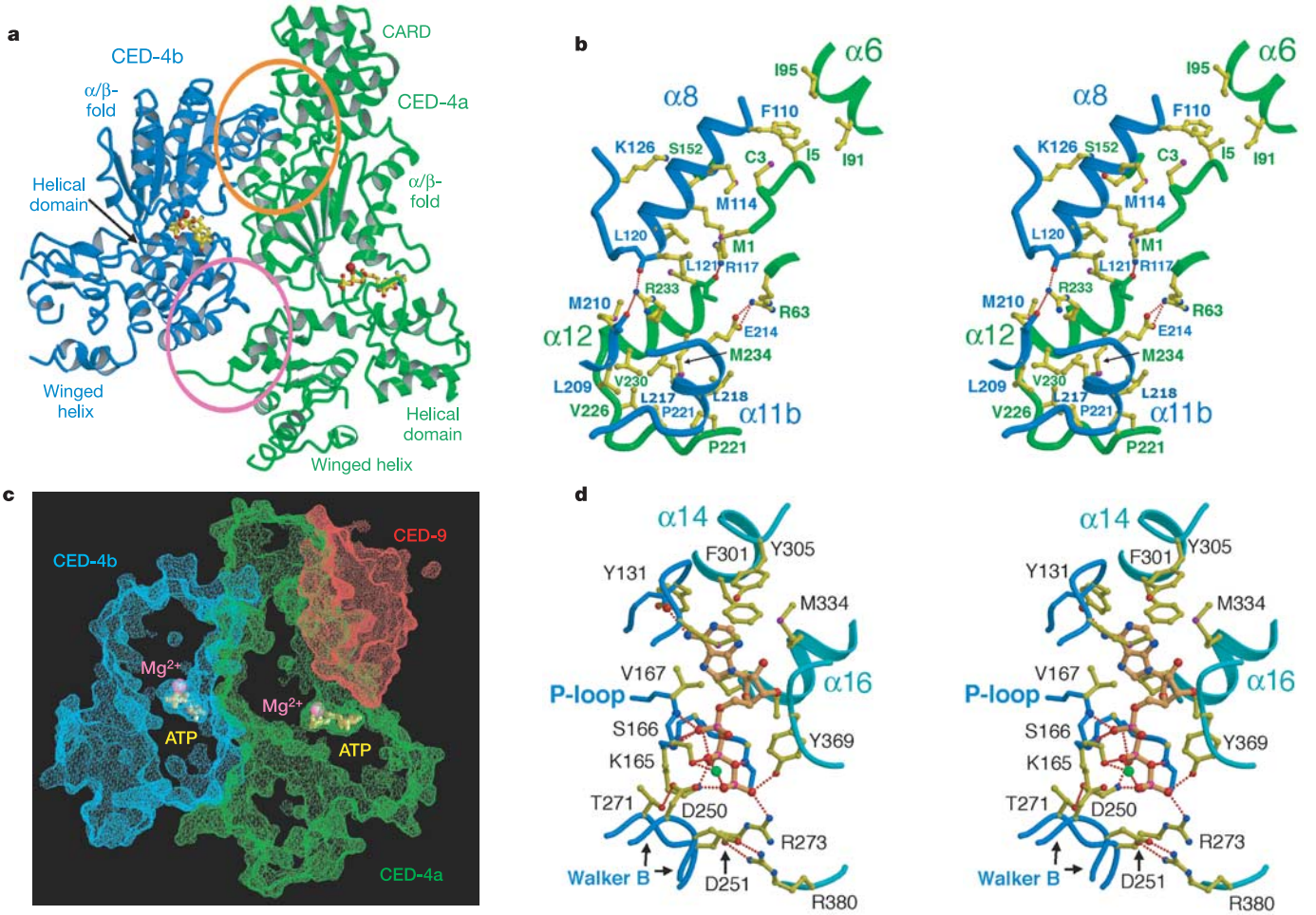

Figure 3 | Structural analyses of the CED-4a–CED-4b interface and ATP binding. **a**, The CED-4a–CED-4b interactions consist of a primary (orange circle) and a secondary (magenta circle) site. **b**, A stereo view of the primary interface of the CED-4 dimer. Helices α8, α11 and α11b, from CED-4b, stack against the CARD and α/β domains of CED-4a. **c**, ATP and magnesium are buried in CED-4. ATP molecules and magnesium ions are highlighted in yellow and magenta, respectively. **d**, A stereo view of ATP coordination in CED-4. Hydrogen bonds are represented by red dashed lines. ATP is shown in orange, with nitrogen and oxygen atoms shown in blue and red, respectively.

facilitate the autoactivation of CED-3 (Fig. 5c). Under conditions where there was no detectable autoprocessing of CED-3 (Fig. 5c, lane 1), the autoactivation of the CED-3 zymogen was accelerated progressively with increasing amounts of CED-4 (Fig. 5c, lanes 2–6). This observation suggests that CED-4 alone is sufficient to promote CED-3 autoactivation.

Next, we examined the role of CED-9 on CED-4-mediated CED-3 activation (Fig. 5d). Under conditions where CED-4 promoted CED-3 maturation (Fig. 5d, lane 1), increasing amounts of CED-9 led to a progressive reduction of CED-3 autoactivation (Fig. 5d, lanes 2–5). Excess CED-9 completely suppressed the positive effect of CED-4 on CED-3 maturation (Fig. 5d, lane 5), reducing the amount of CED-3 cleavage to basal levels (Fig. 5d, lane 6). This result indicates that the anti-apoptotic function of CED-9 is not limited to passively sequestering CED-4 to mitochondria, but also to actively safeguard against CED-4-mediated CED-3 autoactivation. CED-9 does so by trapping an asymmetric dimer of CED-4 and preventing its further dimerization into a tetramer. In further support of this conclusion, incubation of the CED-4 tetramer with CED-9 led to the dissociation of the CED-4 tetramer and formation of the 2:1 CED-4–CED-9 complex (data not shown).

Finally, we assessed whether EGL-1 can counter CED-9-mediated inhibition of CED-4 (Fig. 5e). Under conditions where a stoichiometric complex of CED-4–CED-9 was unable to facilitate CED-3 maturation (Fig. 5e, lanes 1 and 2), incubation with increasing amounts of EGL-1 resulted in a progressive enhancement of CED-3 autoprocessing (Fig. 5e, lanes 3–6) due to the release of CED-4 from the inhibitory CED-4–CED-9 complex. Together, these assays have reconstituted the linear CED-3 activation pathway (Fig. 1a) using the recombinant homogeneous proteins CED-4, CED-9 and EGL-1. Our observations show that the genetically defined pathway is biochemically complete. The observed effects are specific, because neither CED-9 nor EGL-1 alone exhibited any effect on CED-3 maturation (Fig. 5f, lanes 3 and 4).

The reconstituted CED-3 activation assay provides us with a useful system to understand the mechanisms of CED-3 activation. The CED-4 mutant (CED-4*; V230D-R233E-M234E), which formed a 1:1 complex with CED-9 (Supplementary Fig. 3a; Fig. 4a, pink dashed line), is exclusively monomeric in solution (Fig. 4a, green line). This mutant was unable to facilitate CED-3 autoactivation (Fig. 5g, lane 3). These observations suggest that the interface of the asymmetric CED-4 dimer is essential for the formation of the CED-4 tetramer, and for the subsequent induction of CED-3 autoactivation.

The CED-4* mutant (V230D-R233E-M234E) forms a stable dimer with another CED-4 mutant (CED-4″; L209E-L217E-L218E) that contains mutations on a different surface patch (Fig. 4a, purple line). This mutant CED-4 dimer is unable to dimerize further, suggesting that these mutations affect residues that are directly involved in CED-4 tetramerization, and thus are unlikely to affect interaction with CED-3. This mutant CED-4 dimer is also unable to facilitate the autoactivation of CED-3 (Fig. 5g, lane 5). Taken together, our data further suggest that only the wild-type CED-4 tetramer, but not a CED-4 dimer, is capable of mediating CED-3 autoactivation. These observations provide a mechanistic explanation as to why CED-9-sequestered CED-4 is unable to facilitate CED-3 autoactivation.

To examine the effect of CED-4 mutation *in vivo*, we introduced transgenes that expressed various CED-4 mutants, under the control of an endogenous *ced-4* promoter, into *ced-1(e1735);ced-4(n1162)* animals and examined whether they could rescue the *ced-4* cell-death-defective phenotype. No cell corpses were observed in *ced-1(e1735);ced-4(n1162)* animals, as the *ced-4(n1162)* mutation prevents almost all cell deaths. The wild-type *ced-4* transgene was able to restore cell killing in these animals (Supplementary Table 2). In contrast, the monomeric CED-4* mutant (V230D-R233E-M234E) induced very few cell deaths, indicating a loss of *ced-4* rescue activity. Other CED-4 mutants, with compromised abilities to form tetramers *in vitro*, also showed reduced capacities to induce cell death.

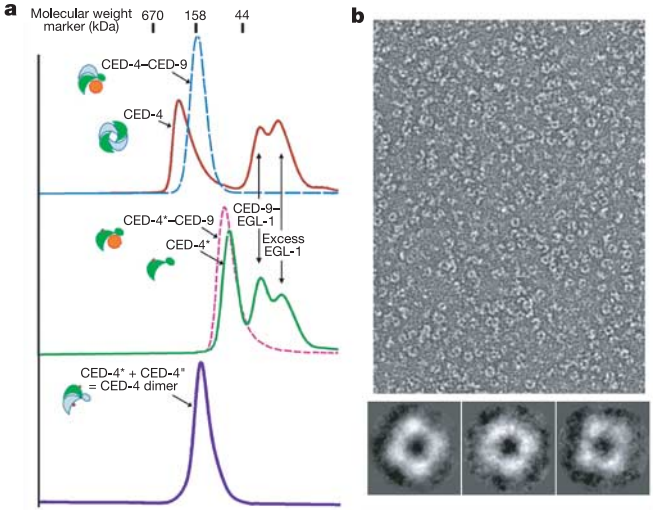

Figure 4 | Free CED-4 forms a tetramer. a, Free CED-4 appears to form a tetramer, as determined by gel filtration. Incubation of the CED-4–CED-9 complex (blue dashed line) with excess EGL-1 resulted in the release of CED-4 and formation of the EGL-1–CED-9 complex (red line). The mutant CED-4* (V230D-R233E-M234E) formed a 1:1 complex with CED-9 (pink dashed line) and is exclusively monomeric (green line). CED-4* and CED-4″ (L209E-L217E-L218E) only formed a dimer (purple line). **b**, Electron microscopy reveals a tetrameric organization for free CED-4. A raw electron micrograph (×30,000) and three class averages of the CED-4 particle are shown.

Discussion

Our study provides mechanistic explanations to published observations on the interaction of CED-4 with CED-9. CED-4L, a splicing variant of CED-4, inhibits programmed cell death[30]. Compared with wild-type CED-4, CED-4L contains an insertion of 24 amino acids after Lys 212 at the centre of the CED-4a–CED-4b interface, and hence is predicted to disrupt this interaction. Therefore, CED-4L is unlikely to form a tetramer, and thus would be unable to mediate CED-3 autoactivation. Moreover, CED-4L (as CED-4a) can still form a dimer with wild-type CED-4 (as CED-4b). This would constitute dominant-negative regulation of wild-type CED-4, because wild-type CED-4 would be sequestered as a dimer and unable to facilitate CED-3 autoactivation. Finally, the regions surrounding Lys 212 have an important role in binding to CED-9, explaining the observation that CED-4L binds only weakly to CED-9 (ref. 31).

Neither CED-9-bound CED-4 dimer nor free CED-4 tetramer showed any detectable ATPase activity (data not shown), suggesting that ATP and magnesium only play a structural role in these complexes. This notion is supported by mass spectroscopic analysis, which only identified ATP, but not ADP, in both CED-9-bound CED-4 and free tetrameric CED-4. Thus, in contrast to Apaf-1, neither CED-9-bound CED-4 nor EGL-1-released CED-4 is an ATPase, and ATP hydrolysis does not seem to play a part in CED-3 activation in our *in vitro* assays. Nonetheless, we cannot rule out the possibility that an additional cofactor may help CED-4 to hydrolyse ATP *in vivo*, which further regulates CED-4 activity.

In summary, our study provides important insights into the regulation of cell death activation in *C. elegans*. In healthy cells, the CED-4 dimer is sequestered by CED-9 at mitochondria, and is unable to facilitate the autoactivation of CED-3 (Fig. 5h). At the onset of cell death, EGL-1 binds to, and triggers a conformational change in, CED-9, resulting in the release of CED-4 from the inhibitory CED-4–CED-9 complex. The released CED-4 dimer

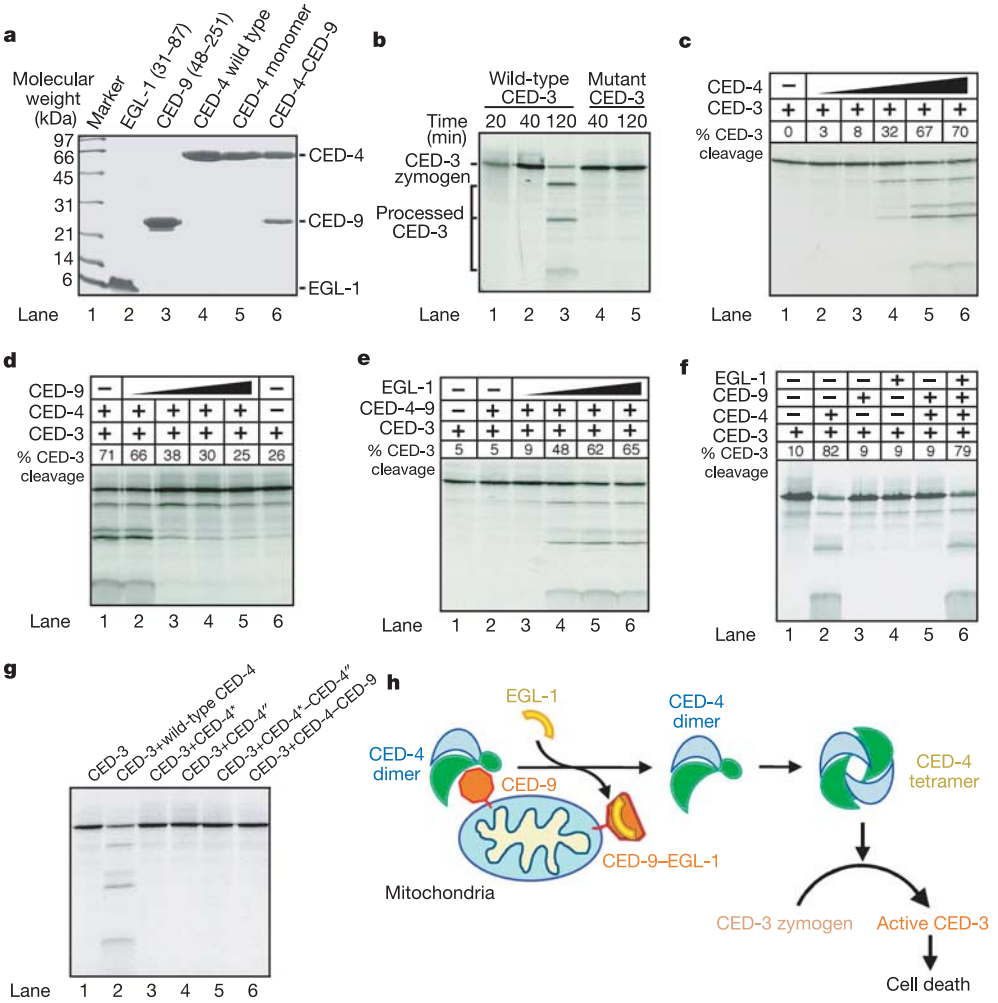

Figure 5 | Complete reconstitution of the CED-3 activation pathway using homogeneous proteins of CED-4, CED-9 and EGL-1. **a**, A representative SDS–PAGE gel (stained by Coomassie blue) showing the recombinant proteins. **b**, ^{35}S-labelled *in vitro* translated wild-type, but not C358S mutant, CED-3 zymogen was autoprocessed. **c**, Recombinant CED-4 protein facilitated the autoactivation of CED-3 in a concentration-dependent manner. Increasing amounts (0.1, 0.5, 2.5, 10 and 50 ng) of CED-4 (lanes 2–6) were used. **d**, Recombinant CED-9 protein inhibited CED-4-mediated autoactivation of CED-3 in a concentration-dependent manner. Increasing amounts (5, 25, 100 and 500 ng) of CED-9 (lanes 2–5) and 50 ng of CED-4 were used. **e**, Recombinant EGL-1 protein countered CED-9-mediated inhibition in a concentration-dependent manner. Increasing amounts (1, 5, 20 and 100 ng) of EGL-1 (lanes 3–6) and 50 ng of CED-4–CED-9 were used. **f**, Complete reconstitution of the CED-3 activation pathway, using 50 ng of each recombinant protein. **g**, Formation of a CED-4 tetramer is required for CED-3 autoactivation. Neither the monomeric CED-4* mutant nor the dimeric CED-4*–CED-4″ mutant complex was able to facilitate the autoactivation of CED-3. Again, 50 ng of each recombinant protein was used. **h**, A schematic diagram of the cell death pathway leading to CED-3 activation.

undergoes further dimerization to form a tetrameric CED-4 complex, which is responsible for the induction of CED-3 autoactivation.

METHODS

Protein preparation. All constructs were generated using a standard polymerase chain reaction-based cloning strategy. CED-4 and CED-9 were coexpressed in the bacterial strain BL21 (DE3) using the vectors pBB75 and pET-15b (Novagen). CED-9 contained a 6 × His tag at its N terminus, and CED-4 was untagged. The bacterial growth temperature for soluble protein expression was optimized at 15 °C. Proteins were purified to homogeneity as described[20].

Crystallization and data collection. Crystals of the CED-4–CED-9 complex were grown at 22 °C using the hanging drop vapour diffusion method. The well buffer contained 0.1 M HEPES, pH 7.5, 20% (w/v) PEG 3350 and 0.2 M $(NH_4)_2SO_4$. The crystals grew to full size within 12 h, with a typical dimension of 0.3 × 0.3 × 0.8 mm^3. The crystals belong to the space group $P4_12_12$ and contain one complex per asymmetric unit. The unit cell has dimensions of $a = b = 128.9$ Å, $c = 209.9$ Å. Selenomethionine (SeMet)-labelled protein complex was crystallized under the same conditions. Native and anomalous diffraction data were collected at the National Synchrotron Light Source (NSLS) beamline X-25. The data sets were collected at 100 K and processed using the HKL2000 software suite[32].

Structure determination. The CED-4–CED-9 complex structure was solved by MAD phasing. At 5.0 Å resolution, 39 Se sites were found using the program SHELXD (ref. 33). Using the peak-wavelength data at 4.0 Å resolution, the correct handedness of the Se substructure was identified by the program ABS (ref. 34) and further refined using SOLVE (ref. 35), resulting in a figure of merit of 0.52 for all reflections within 3.1 Å. Combined with the native data, the 3.1 Å MAD phases were gradually extended to 2.6 Å by solvent flipping implemented in the program SOLOMON (ref. 36). The electron density map at 2.6 Å is of excellent quality and allows the model to be built in program O (ref. 37). The atomic model was refined using CNS (ref. 38).

Electron microscopy and image analysis. For electron microscopy, 5 µl of CED-4 sample, at a concentration of 0.1 mg ml^{-1} in 10 mM Tris, pH 8.0, 40 mM NaCl and 2 mM dithiothreitol (DTT), was transferred to a freshly glow-discharged 300-mesh copper grid covered with a thin layer of carbon film. The grid was then blotted and stained with a 5 µl drop of 2% uranyl acetate aqueous solution. The stain solution was blotted after 1 min, and the grid was left to air-dry. The grids were imaged in a JEOL 1200EX transmission electron microscope operated at 120 kV. Electron micrographs were recorded on Kodak SO-163 negative film at a magnification of ×30,000. After digitizing the film

with a Nikon SuperCool scanner, ~9,500 particles were non-discriminatorily selected from the raw images. All particle images were classified through a multivariant statistical analysis. Particles belonging to the same classes were averaged to provide statistically better-defined views.

***In vitro* CED-3 activation assay.** Wild-type full-length CED-3 was translated using the TNT T7 quick coupled transcription and translation system (Promega) at 30 °C for 25 min. The indicated proteins (CED-4 and its mutants, CED-9 and EGL-1) were added to the translation product in a 20 μl volume and incubated at 30 °C for another 25 min before samples were analysed by SDS–polyacrylamide gel electrophoresis (SDS–PAGE) and autoradiography. The extent of CED-3 cleavage, defined by the intensity ratio of cleaved CED-3 over total CED-3, was quantified using the EagleEye system (Stratagene).

Gel filtration assays. For each assay, 500 μl of purified wild-type or mutant CED-4–CED-9 complex, with or without EGL-1, was applied to Superdex 200 (Amersham) in buffer containing 25 mM HEPES, pH 8.0, 150 mM NaCl and 2 mM DTT. The peak fractions were analysed by SDS–PAGE and visualized by Coomassie blue staining.

Isothermal titration calorimetry. To obtain a direct binding affinity between CED-9 and CED-4, 0.1 mM CED-9 (residues 48–251) was titrated against 9 μM CED-4 monomer mutant using a VP-ITC microcalorimeter (MicroCal). To assess the ability of EGL-1 to dissociate CED-9 from the wild-type CED-4–CED-9 complex, 0.26 mM EGL-1 (residues 31–87) was titrated against 14 μM wild-type CED-4–CED-9 complex. All proteins were prepared in a buffer containing 25 mM HEPES, pH 8.0, and 150 mM NaCl. The data were fitted using the software Origin 7.0 (MicroCal).

***ced-4* rescue assays.** *ced-1(e1735);ced-4(n1162);unc-76(e911)* animals were injected with a *ced-4* construct at 50 ng μl^{-1}, along with the injection markers pTG96 (P*sur-5*::GFP) and p7616B (*unc-76* rescue plasmid) each at 20 ng μl^{-1}. Cell corpses were scored in the anterior head region of 1.5-fold and 4-fold transgenic fluorescent embryos. At least ten animals were scored for each transgenic line.

Received 7 April; accepted 4 July 2005.

1. Horvitz, H. R. Worms, Life, and Death (Nobel Lecture). *ChemBioChem* **4,** 697–711 (2003).
2. Horvitz, H. R. Genetic control of programmed cell death in the nematode *Caenorhabditis elegans*. *Cancer Res.* **59,** 1701–1706 (1999).
3. Yuan, J., Shaham, S., Ledoux, S., Ellis, H. M. & Horvitz, H. R. The *C. elegans* cell death gene *ced-3* encodes a protein similar to mammalian interleukin-1β-converting enzyme. *Cell* **75,** 641–652 (1993).
4. Xue, D., Shaham, S. & Horvitz, H. R. The *Caenorhabditis elegans* cell-death protein CED-3 is a cysteine protease with substrate specificities similar to those of the human CPP32 protease. *Genes Dev.* **10,** 1073–1083 (1996).
5. Thornberry, N. A. & Lazebnik, Y. Caspases: Enemies within. *Science* **281,** 1312–1316 (1998).
6. Yuan, J. & Horvitz, H. R. The *Caenorhabditis elegans* cell death gene *ced-4* encodes a novel protein and is expressed during the period of extensive programmed cell death. *Development* **116,** 309–320 (1992).
7. Chinnaiyan, A. M., O'Rourke, K., Lane, B. R. & Dixit, V. M. Interaction of CED-4 with CED-3 and CED-9: a molecular framework for cell death. *Science* **275,** 1122–1126 (1997).
8. Irmler, M., Hofmann, K., Vaux, D. & Tschopp, J. Direct physical interaction between the *Caenorhabditis elegans* 'death proteins' CED-3 and CED-4. *FEBS Lett.* **406,** 189–190 (1997).
9. Seshagiri, S. & Miller, L. K. *Caenorhabditis elegans* CED-4 stimulates CED-3 processing and CED-3-induced apoptosis. *Curr. Biol.* **7,** 455–460 (1997).
10. Wu, D., Wallen, H. D. & Nunez, G. Interaction and regulation of subcellular localization of CED-4 by CED-9. *Science* **275,** 1126–1129 (1997).
11. Yang, X., Chang, H. Y. & Baltimore, D. Essential role of CED-4 oligomerization in CED-3 activation and apoptosis. *Science* **281,** 1355–1357 (1998).
12. Hengartner, M. O. & Horvitz, H. R. *C. elegans* cell survival gene *ced-9* encodes a functional homolog of the mammalian proto-oncogene *bcl-2*. *Cell* **76,** 665–676 (1994).
13. Chen, F. *et al.* Translocation of *C. elegans* CED-4 to nuclear membranes during programmed cell death. *Science* **287,** 1485–1489 (2000).
14. James, C., Gschmeissner, S., Fraser, A. & Evan, G. I. CED-4 induces chromatin condensation in *Schizosaccharomyces pombe* and is inhibited by direct physical association with CED-9. *Curr. Biol.* **7,** 246–252 (1997).
15. Spector, M. S., Desnoyers, S., Hoeppner, D. J. & Hengartner, M. O. Interaction between the *C. elegans* cell-death regulators CED-9 and CED-4. *Nature* **385,** 653–656 (1997).
16. Conradt, B. & Horvitz, H. R. The *C. elegans* protein EGL-1 is required for programmed cell death and interacts with the Bcl-2-like protein CED-9. *Cell* **93,** 519–529 (1998).
17. del Peso, L., Gonzalez, V. M. & Nunez, G. *Caenorhabditis elegans* EGL-1 disrupts the interaction of CED-9 with CED-4 and promotes CED-3 activation. *J. Biol. Chem.* **273,** 33495–33500 (1998).
18. del Peso, L., Gonzalez, V. M., Inohara, N., Ellis, R. E. & Nunez, G. Disruption of the CED-9·CED-4 complex by EGL-1 is a critical step for programmed cell death in *Caenorhabditis elegans*. *J. Biol. Chem.* **275,** 27205–27211 (2000).
19. Parrish, J., Metters, H., Chen, L. & Xue, D. Demonstration of the *in vivo* interaction of key cell death regulators by structure-based design of second-site suppressors. *Proc. Natl Acad. Sci. USA* **97,** 11916–11921 (2000).
20. Yan, N. *et al.* Structural, biochemical, and functional analyses of CED-9 recognition by the proapoptotic proteins EGL-1 and CED-4. *Mol. Cell* **15,** 999–1006 (2004).
21. Riedl, S. J., Li, W., Chao, Y., Schwarzenbacher, R. & Shi, Y. Structure of the apoptotic protease activating factor 1 bound to ADP. *Nature* **434,** 926–933 (2005).
22. Zou, H., Henzel, W. J., Liu, X., Lutschg, A. & Wang, X. Apaf-1, a human protein homologous to *C. elegans* CED-4, participates in cytochrome c-dependent activation of caspase-3. *Cell* **90,** 405–413 (1997).
23. Holm, L. & Sander, C. Protein structure comparison by alignment of distance matrices. *J. Mol. Biol.* **233,** 123–138 (1993).
24. Liu, J. *et al.* Structure and function of Cdc6/Cdc18: implications for origin recognition and checkpoint control. *Mol. Cell* **6,** 637–648 (2000).
25. Singleton, M. R. *et al.* Conformational changes induced by nucleotide binding in Cdc6/ORC from *Aeropyrum pernix*. *J. Mol. Biol.* **343,** 547–557 (2004).
26. Lupas, A. N. & Martin, J. AAA proteins. *Curr. Opin. Struct. Biol.* **12,** 746–753 (2002).
27. Jaroszewski, L., Rychlewski, L., Reed, J. C. & Godzik, A. ATP-activated oligomerization as a mechanism for apoptosis regulation: fold and mechanism prediction for CED-4. *Proteins* **39,** 197–203 (2000).
28. Woo, J. S. *et al.* Unique structural features of a BCL-2 family protein CED-9 and biophysical characterization of CED-9/EGL-1 interactions. *Cell Death Differ.* **10,** 1310–1325 (2003).
29. Hugunin, M., Quintal, L. J., Mankovich, J. A. & Ghayur, T. Protease activity of *in vitro* transcribed and translated *Caenorhabditis elegans* cell death gene (*ced-3*) product. *J. Biol. Chem.* **271,** 3517–3522 (1996).
30. Shaham, S. & Horvitz, H. R. An alternatively spliced *C. elegans ced-4* RNA encodes a novel cell death inhibitor. *Cell* **86,** 201–208 (1996).
31. Ottilie, S. *et al.* Mutational analysis of the interacting cell death regulators CED-9 and CED-4. *Cell Death Differ.* **4,** 526–533 (1997).
32. Otwinowski, Z. & Minor, W. Processing of X-ray diffraction data collected in oscillation mode. *Methods Enzymol.* **276,** 307–326 (1997).
33. Uson, I. & Sheldrick, G. M. Advance in direct methods for protein crystallography. *Curr. Opin. Struct. Biol.* **9,** 643–648 (1999).
34. Hao, Q. ABS: A program to determine absolute configuration and evaluate anomalous scatter substructure. *J. Appl. Crystallogr.* **37,** 498–499 (2004).
35. Terwilliger, T. C. & Berendzen, J. Automated structure solution for MIR and MAD. *Acta Crystallogr. D* **55,** 849–861 (1999).
36. Abrahams, J. P. & Leslie, A. G. Methods used in the structure determination of bovine mitochondrial F1 ATPase. *Acta Crystallogr. D* **52,** 30–42 (1996).
37. Jones, T. A., Zou, J.-Y., Cowan, S. W. & Kjeldgaard, M. Improved methods for building protein models in electron density maps and the location of errors in these models. *Acta Crystallogr. A* **47,** 110–119 (1991).
38. Brunger, A. T. *et al.* Crystallography and NMR System: A new software suite for macromolecular structure determination. *Acta Crystallogr. D* **54,** 905–921 (1998).
39. Kraulis, P. J. MOLSCRIPT: a program to produce both detailed and schematic plots of protein structures. *J. Appl. Crystallogr.* **24,** 946–950 (1991).
40. Nicholls, A., Sharp, K. A. & Honig, B. Protein folding and association: insights from the interfacial and thermodynamic properties of hydrocarbons. *Proteins Struct. Funct. Genet.* **11,** 281–296 (1991).

Supplementary Information is linked to the online version of the paper at www.nature.com/nature.

Acknowledgements We thank H. R. Horvitz for complementary DNA sequences of *egl-1*, *ced-9*, *ced-4* and *ced-3*, and for his encouragement. We thank V. Dixit and X. Yang for providing *ced-3* constructs, and M. Becker and A. Saxena for beamtime at NSLS. This research was supported by NIH grants to Y.S. and D.X. H.L. acknowledges support from the Brookhaven National Laboratory LDRD program and a Department of Energy grant. The atomic coordinates of the CED-4–CED-9 complex have been deposited in the Protein Data Bank with the accession number 2A5Y.

Author Contributions N.Y. performed the bulk of the experiments. N.Y. and Y.S. designed and interpreted the bulk of the experiments. J.C., E.S.L., L.G., Q.L., J.H., J.-W.W. and D.K. contributed to experiments. J.C., E.S.L., L.G., Q.L., J.H., J.-W.W., D.K., H.L., Q.H. and D.X. contributed to data analysis and interpretation. N.Y. and Y.S. wrote the paper. J.C. and E.S.L. contributed equally to this work.

Author Information Reprints and permissions information is available at npg.nature.com/reprintsandpermissions. The authors declare no competing financial interests. Correspondence and requests for materials should be addressed to Y.S. (yshi@molbio.princeton.edu).